Available online at www.sciencedirect.com
SCIENCE DIRECT®
Journal of Solid State Chemistry 179 (2006) 804–811
JOURNAL OF SOLID STATE CHEMISTRY
www.elsevier.com/locate/jssc

Synthesis, characterization, and photocatalytic properties of $InVO_4$ nanoparticles

Liwu Zhang, Hongbo Fu, Chuan Zhang, Yongfa Zhu*

Department of Chemistry, Tsinghua University, Beijing 100084, PR China

Received 9 October 2005; received in revised form 30 November 2005; accepted 1 December 2005
Available online 6 January 2006

Abstract

Nanosized $InVO_4$ with orthorhombic structure was successfully synthesized at a relatively low calcination temperature of 600 °C by using an amorphous heteronuclear complex as precursor. The photocatalytic activity of $InVO_4$ catalyst has been evaluated by the decomposition of formaldehyde (FAD) under UV light ($\lambda = 254$ nm) and visible light irradiation ($\lambda > 420$ nm). The as-synthesized $InVO_4$ catalyst showed higher photocatalytic activity for the FAD decomposition compared to the sample prepared by the conventional solid-state reaction. The calculations of the electronic band structures indicated that the valence band was composed of the O 2*p* orbitals, whereas the conduction band was formed by the V 3*d* orbitals with a small contribution of the In 5*s* orbitals. The photocatalytic activity of the as-prepared sample is discussed on the basis of the electronic band structure and bulk material structure.
© 2005 Elsevier Inc. All rights reserved.

Keywords: $InVO_4$; Nano-crystalline; Photocatalysis; Visible light

1. Introduction

In the past three decades, many investigations have been focused on the TiO_2 photocatalyst because of its high activity and chemical stability [1–4]. However, the band gap of TiO_2 is above 3.0 eV, it is only active under ultraviolet (UV) irradiation. In order to improve the efficiency of utilizing the solar energy, many researches are focused on the development of the new visible-light-induced photocatalysts, and some complex oxides have been found to have the visible light driven catalytic activity, such as $BiVO_4$ [5,6], $In_{1-x}Ni_xTaO_4$ ($x = 0 - 0.2$) [7], $RbLnTa_2O_7$ (Ln = La, Pr, Nd, and Sm) [8], $MIn_{0.5}Nb_{0.5}O_3$ (M = Ca, Sr, and Ba) [9], $CaIn_2O_4$ [10], etc.

Recently, it has also been reported that $InVO_4$ is a good photocatalyst for water splitting under visible light irradiation [11–13]. However, $InVO_4$ was usually prepared by the solid-state reactions, which needed high temperature, long reaction time. Moreover, the sizes of the photocatalysts were often situated in micro-scale and the activities were still relative low. Therefore, developing of new routes to obtain $InVO_4$ with high surface area is necessary to improve the photocatalytic activity.

Several methods have been developed to synthesize $InVO_4$, such as the classical ceramic route from In_2O_3 and V_2O_5 [14], 'chimie douce' approach [15], and precipitation of the aqueous solution of $InCl_3$ and NH_4VO_3 [16], etc. Nanosized particles and thin films are not easily obtained by these traditional methods. With regard to the particle size, nanostructured materials are usually better for photocatalysis due to high surface area and quantum effects [17–19] .The sol–gel method has been widely used to prepare nanosized materials, but its application is limited by the stability of its precursor system and it is difficult to control the chemical composition of complex oxides [20].

In this work, nanosized $InVO_4$ was prepared by using an amorphous heteronuclear complex as a precursor. It is well known that this method was suitable to prepare the certain materials at relatively low temperature. Especially, It was easy to prepare film materials using this method [21–24]. The crystalline phase of $InVO_4$ with an orthorhombic structure can be obtained after the precursor is calcined at 600 °C. The temperature is almost 500 °C lower than that

*Corresponding author. Fax: +86 10 62787601.
E-mail address: zhuyf@mail.tsinghua.edu.cn (Y. Zhu).

0022-4596/$ - see front matter © 2005 Elsevier Inc. All rights reserved.
doi:10.1016/j.jssc.2005.12.003

of classic method [14]. The photocatalytic activity for the formaldehyde (FAD) decomposition was then compared to a sample prepared by the conventional solid-state reaction technique.

2. Experiments

2.1. Synthesis of the precursor

Commercial In_2O_3 or $In(OH)_3$ were often stable and could not dissolve in general inorganic acid or organic acid (except HF). In contrast, freshly precipitated $In(OH)_3$ was highly active species, which could dissolve in strong alkali and some hot organic acid, such as excess hot citric acid. Preparing of freshly precipitated $In(OH)_3$ was similar to Judit's method [25]. A 2.5 g In_2O_3 (9 mmol) was dissolved in HCl solution and then added excess ammonium solution to prepare the fresh $In(OH)_3$ precipitate. The precipitate was centrifugated from the solution and washed with distilled water several times.

The 13.61 g of diethylenetriaminepentaacetic acid (DTPA) was dissolved in 50 mL distilled hot water. Then both the V_2O_5 and fresh $In(OH)_3$ precipitate were added to the hot DTPA solution. The mixture was stirred and heated to 80 °C to promote the reaction of the mixture. After the mixture became a transparent solution, it was vaporized slowly at room temperature until a piece of transparent glasslike material was formed. The precursor was obtained after the solution was dried completely.

Nano-sized orthorhombic $InVO_4$ was synthesized by calcining the precursor in air. A slow heating rate (3 °C/min) was used to increase temperature to various pre-set temperatures and maintained for a definite period of time to promote the formation of cobaltite oxide. Meanwhile, $InVO_4$ were synthesized by traditional solid-state reaction according to Ref. [14] for comparison with the nanoparticles.

2.2. Analysis techniques

TGA-DTA analyses were performed on a Dupont 1090 thermal analyzer. The atmosphere was air and the heating rate was 5 °C/min. X-ray diffraction (XRD) experiments were carried out using a Rigaku DMAX-2400 diffractometer with Cu$K\alpha$ radiation. The average crystal size was determined from the XRD pattern parameters according to the Scherrer equation: $D_c = K\lambda/\beta \cos\theta$. D_c is the average crystal size, K is the Scherrer constant equal to 0.89, β is the full-width at half-maximum (FWHM) and θ is the diffraction angle. The peak at 33.1° was used for the calculation of the crystal size, because it had relatively strong intensity and did not overlap with the other diffraction peaks. The grain size was measured using a Hitachi H-800 transmission electron microscope (TEM). The accelerating voltage of electron beam was 200 kV. UV–Vis diffuse reflectance spectrums (DRS) of the samples were measured by using Hitachi U-3010 UV–Vis spectrophotometer.

2.3. Photocatalytic reactions

The visible light photocatalytic activities of $InVO_4$ nanoparticles were evaluated by the decomposition of FAD. The optical system for the photocatalytic reaction was composed of a 500 W Xe arc lamp and a cutoff filter ($\lambda > 420$ nm). The average light intensity was 31 mW cm^{-2}. The photoreactor used was a 400 mL cylindrical quartz vessel, which consisted of an inlet, an outlet and a sample port. A 0.1 g $InVO_4$ powders of each preparing condition were dispersed in about 1 mL ethanol. The solution was dripped onto clean glass slide and was made to spread on the slide uniformly. When the solution was evaporated, a coated slide was generated. The blank glass slide or coated slide was tested in the vessel perpendicular to the light beam. The area of the glass slide was 7.5×2.5 cm. The distance between the film and the light source was 10 cm, where the light intensity was measured to be 31 mW cm^{-2}. A mixture which contains FAD of about 1800 ppm was then forced into the photoreactor. Then the photoreactor was sealed and photocatalytic reaction was started by turning on the UV-lamp. The concentration of FAD was measured by a SP-502 gas chromatograph (GC) equipped with a flame ionization detector and a 2 m stainless steel column (GDX-403) at 373 K.

A UV-light lamp of 11 W ($\lambda = 254$ nm, Institute of Electric Light Source, Beijing) was used to provide the UV-light-source. The distance between the film and the light source was 5 cm, where the light intensity was measured to be 120 μW/cm^2.

3. Results and discussion

3.1. Thermal decomposition process

To understand the formation mechanism of $InVO_4$, thermogravimetric analysis (TGA) and differential thermal analysis (DTA) were performed on the as-synthesized amorphous precursor. The results of TGA and DTA for the precursor are shown in Fig. 1. The change of residual

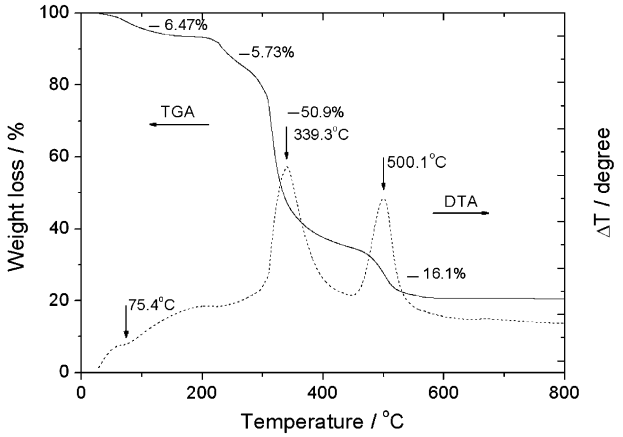

Fig. 1. The TGA and DTA spectrum of the precursor.

weight with temperature was shown by the solid curve and the thermal change with temperature was shown by the dot curve. With the temperature rising, four weight loss regions were observed in the solid curve. Based on the quantitative calculation of the weight loss in each region, the thermal decomposition processes were distinguished as followings. The weight loss region from 20 to 130 °C resulted from the loss of coordinated water, hence the amount of coordination water can be estimated. The region of weight loss from 130 to 240 °C was attributed to the decomposition of hydrocarbon and amino-group organic components. A notable weight loss region from 240 to 410 °C was attributed to the decomposition of carboxyl indium group. The other notable region of weight loss from 410 to 580 °C was attributed to the decomposition of carboxyl vanadium group. No further peak or weight loss appears thereafter, indicating that all organic components have been eliminated. There are three features in the DTA curve. At approximately 75.4 °C, a small endothermic peak is observed. This peak is attributed to the removal of residual and coordinated water. Two obvious exothermic peaks were observed on the DTA curve. The peak at 339.3 °C was attributed to the decomposition of carboxyl indium group. The peak at 500.1 °C resulted from the decomposition of carboxyl vanadium group and the formation of the $InVO_4$ complex. This result suggests that the formation of the $InVO_4$ oxide occurred at 500 °C by decomposing an amorphous complex.

3.2. Crystallization of $InVO_4$ photocatalysts

The influence of the calcination temperature on the formation of $InVO_4$ crystalline phase has been investigated by XRD. The XRD patterns of the $InVO_4$ samples calcined at different temperature are shown in Fig. 2. After the precursor was calcined at 500 °C, the XRD pattern showed that the sample was still amorphous. Characteristic peaks of crystalline phase were observed after the precursor was calcined at 550 °C, the marked peaks in Fig. 2 are due to certain intermediates. Sharper peaks were observed after the precursor was calcined at 600 °C. According to the XRD standard spectra of $InVO_4$ crystal, these peaks were attributed to the orthorhombic $InVO_4$ phase. This result indicated that $InVO_4$ with pure orthorhombic structure can be synthesized by this method above 600 °C, which is consistent with the TGA-DTA result. The formation of $InVO_4$ significantly depend on the thermal decomposition process of the precursor, it is illuminated in Fig. 1 that the decomposition of carboxyl group was completed till 580 °C, and at 500 °C there were still lots of organic groups in the precursor, no diffraction peaks were observed in the XRD patterns, the catalyst was still amorphous. At 600 °C, as all organic components have been eliminated, $InVO_4$ with orthorhombic phase formed. With the increase of the calcination temperatures, the peak intensity did not change significantly, indicating that the crystalline phase of $InVO_4$ did not grow with the calcination temperature.

The influence of calcination time on the formation of $InVO_4$ crystalline phase at 600 °C was also observed by XRD. As shown in Fig. 3, the orthorhombic crystalline phase has formed when the precursor was calcined at 600 °C for 1 h, accompanied with some tiny peaks due to In_2O_3 ($2\theta = 30.8°$). The In_2O_3 peaks disappeared with the increase of the calcination time to 10 h. The peaks were intensified and became sharper with increasing calcination time. This result shows that long calcination time was favorable to the formation of $InVO_4$ crystals.

Comparing with the traditional solid-state reaction method, the formation temperature of $InVO_4$ can decrease from 1100 to 600 °C by using DTPA complex as a precursor. Furthermore, the calcination temperature and time had weak effect on the growth of $InVO_4$ crystalline, indicating that this is an effective method for the preparation of nanosized vanadates.

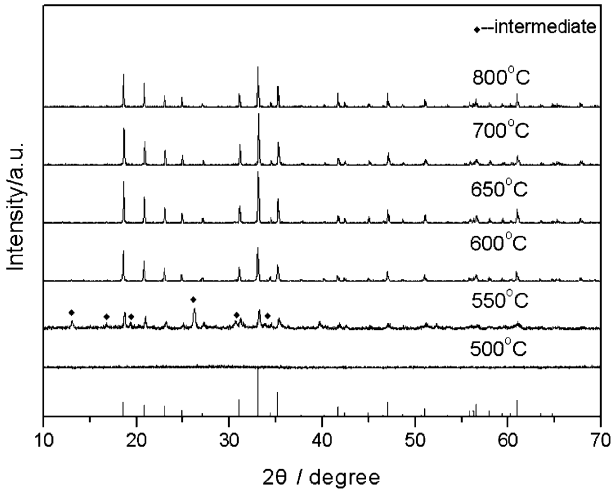

Fig. 2. XRD patterns of $InVO_4$ calcined at different temperatures for 10 h.

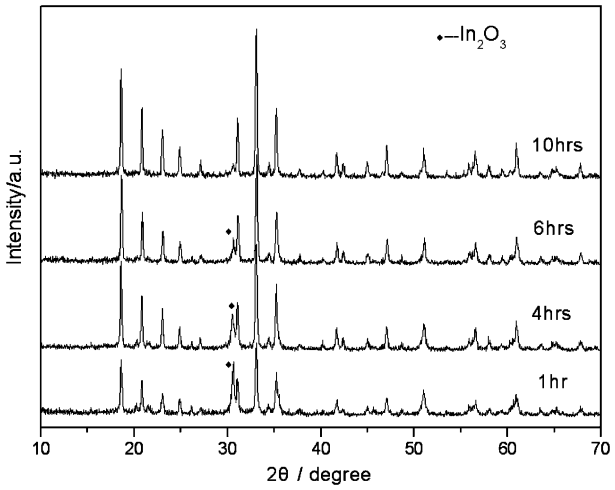

Fig. 3. XRD patterns of $InVO_4$ calcined at 600 °C for different time.

3.3. Grain size and crystal size of $InVO_4$ photocatalysts

The grain size of the $InVO_4$ catalyst varied with calcination temperature and time has been studied by using TEM, as shown in Fig. 4. The grain edge of the sample calcined at 500 °C was a little dim as Fig. 4a showed. It indicated that the sample was still amorphous at this temperature, which was in accordance with the result of XRD. The images of TEM also showed that the grain size was homogenous and fairly small when the sample was obtained at a lower calcination temperature such as 600 °C (Fig. 4b) and 650 °C (Fig. 4c). The average grain size grew quickly after the precursor was calcined at a much higher temperature. It is shown in Fig. 4d that the grain size was much bigger after the sample was calcined at 700 °C.

The dependence of the average grain size on the heat-treatment time was also investigated at 600 °C. The TEM images show that the heat-treatment time has a less obvious effect on the grain size of the powder. The sample calcined for 1 h had the similar grain size compared to the one for 4 h (Fig. 4e). Even when the sample was calcined for 10 h, the grain size did not change significantly. But it began to aggregate. After it was calcined for 20 h, it resulted in the formation of coarse aggregation (Fig. 4f).

We have also compared the crystal size from XRD using Scherrer methods [26] and the grain size counted from TEM images. The results are shown in Tables 1 and 2. With the increase of the calcination temperature, the grain size increased dramatically, especially under the temperature bigger than 700 °C, and the deviation of the grain size increased. But the crystal size increased slightly. This means that the big grains were composed of several crystallites.

3.4. Photo absorption of $InVO_4$ photocatalyst

The UV–Vis DRSs of $InVO_4$ sintered for various times were compared in Fig. 5. The absorption edge of $InVO_4$

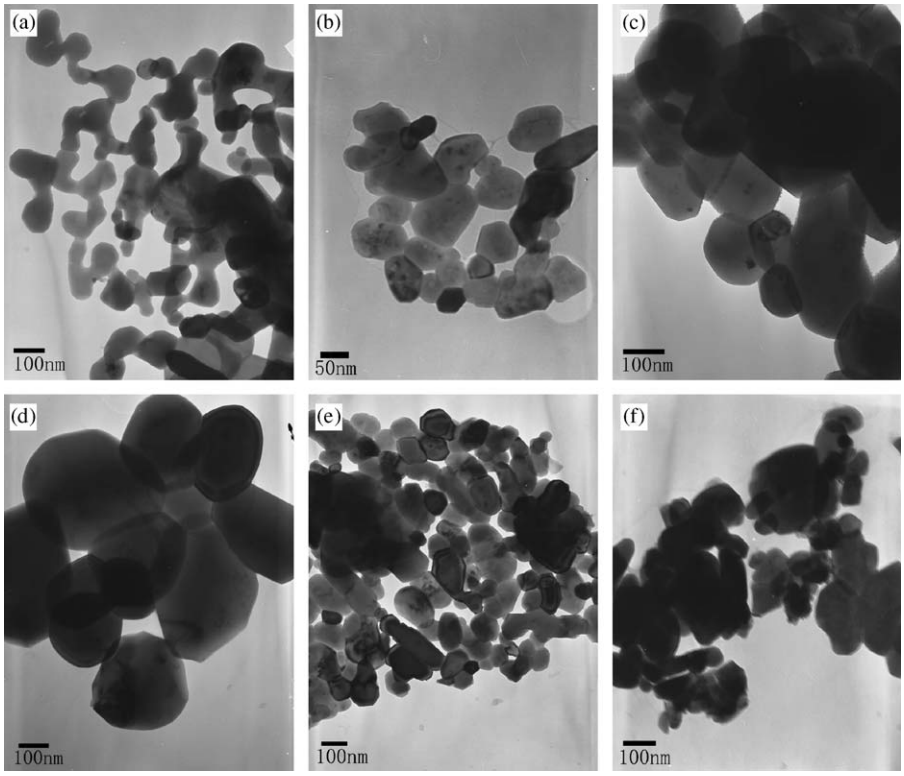

Fig. 4. The TEM photos of the calcined samples: (a) 500 °C for 10 h; (b) 600 °C for 2 h; (c) 650 °C for 10 h; (d) 700 °C for 10 h; (e) 600 °C for 4 h; (f) 600 °C for 20 h.

Table 1
The dependence of grain sizes on the calcination temperature determined from TEM images and the crystal sizes derived from XRD patterns

Temperature/°C for 10 h	500 °C	600 °C	650 °C	700 °C	800 °C	SSR
Average grain size, Dg/nm	40–50	80	100	150–200	300	~1000
Average crystal size, Dc/nm	Amorphous	45.9	48.7	55.6	63.8	86.4

SSR: $InVO_4$ obtained from solid-state reaction.

showed a gradual red shift with increasing calcination time. This is ascribed to the gradual growth of $InVO_4$ crystallites during thermal treatment from 2 to 10 h, as confirmed by the XRD and TEM results (Table 2). The band gap energies estimated from the $(absorbance)^{0.5}(h\nu)^{0.5}$ versus photon energy plots were 1.98, 1.96, 1.94, and 1.90 eV for the $InVO_4$ sintered for 2, 4, 6,10 h, respectively, which coincides with the reported values for $InVO_4$ [11–13].

3.5. Electronic structure calculations

The quantum-mechanical calculations performed here are based on density functional theory (DFT) [27]. Exchange-correlation effects were taken into account by using the generalized gradient approximation (GGA) [28]. The total energy code CASTEP was used [29,30], which utilizes pseudopotentials to describe electron–ion interactions and represents electronic wavefunctions using a plane-wave basis set. The kinetic energy cutoff was set at 280 eV. The Brillouin-zone sampling was performed by using a k-grids of $3 \times 3 \times 3$ points for the calculations.

The calculated band dispersions and densities of states for $InVO_4$ are shown in Fig. 6. The top of the valence band corresponds to orbital ♯42, and the bottom of the conduction band corresponds to orbital ♯43. The contents of each band are shown in Fig. 4. For example, orbitals ♯35–♯42 are composed of O 2p orbitals. The band gap lies between orbitals ♯42 and ♯43. The partial DOS for $InVO_4$ are also shown in Fig. 7 in the energy region from −15 to +10 eV, where the Fermi level is set to zero on the abscissa. The valence band is made up of O 2p, and O 2p + V 3d + In 5s, whereas the conduction band is made up of V 3d orbitals and O 2p orbitals. The conduction band also contains small contributions from In 5s orbitals by the overlap with V 3d orbitals. The band gap is reasonably estimated to be 2.3 eV, taken as the energy difference between the top of the O 2p band and the bottom of the V 3d + O 2p + In 5s band.

The electron density contour map for the band in the middle energy range of valence band is shown in Fig. 8a. Both the O 2p and V 3d orbitals are involved. Fig. 8b is the contour map for the top of valence band (HOMO). The electron density is localized to the O 2p orbitals only. Thus, these results indicate that the lower part consists of the O 2p and V 3d orbitals in the valence band, whereas the upper part is composed of the O 2p orbitals.

The result of electronic structure calculation showed that the conduction band of $InVO_4$ was composed of V 3d hybrid with In 5s, which lowered the energy level of conduction band, and resulted in a narrow band gap energy. Therefore, $InVO_4$ can be driven under visible light irradiation, and indium is one of the candidate elements that are able to make the conduction band lower. This is noteworthy information in order to design new visible-light-driven photocatalysts.

The electronic structure calculations of $InVO_4$ were also reported by Oshikiri et al. [31]. Their calculations based on DFT within the local density approximation (LDA), in the present work, the GGA were used for the exchange-correlation functional. Use of GGA in

Table 2
The dependence of grain sizes on the heat-treatment time determined from TEM photos and the crystal sizes derived from XRD patterns

Heat-treat time/h at 600 °C	1 h	2 h	4 h	6 h	10 h
Average grain size, Dg/nm	40	60	70–80	70–80	80
Average crystal size, Dc/nm	39.8	40.9	41.5	42.6	45.9

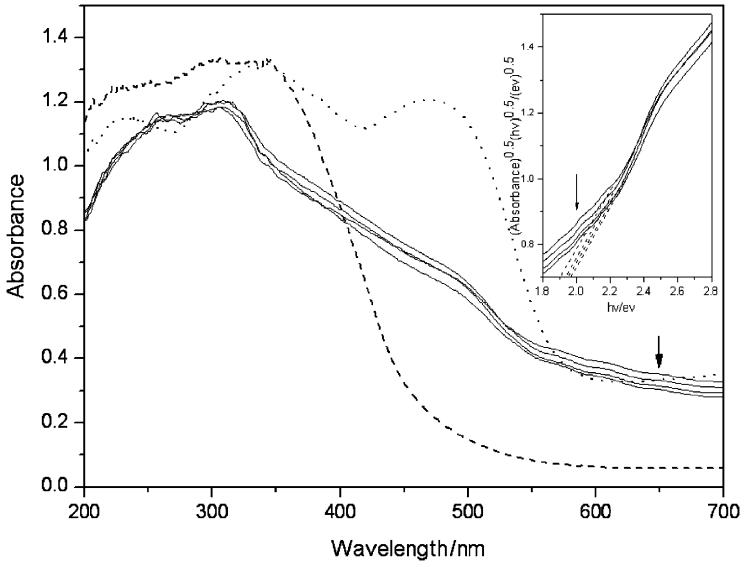

Fig. 5. UV–Vis absorption spectra of the $InVO_4$ catalysts sintered for different times at 600 °C, V_2O_5 (Dot line) and In_2O_3 (Dash line). The inset is plots of $(absorbance)^{0.5}(h\nu)^{0.5}$ versus photon energy, Arrow direction: 2,4,6,10 h.

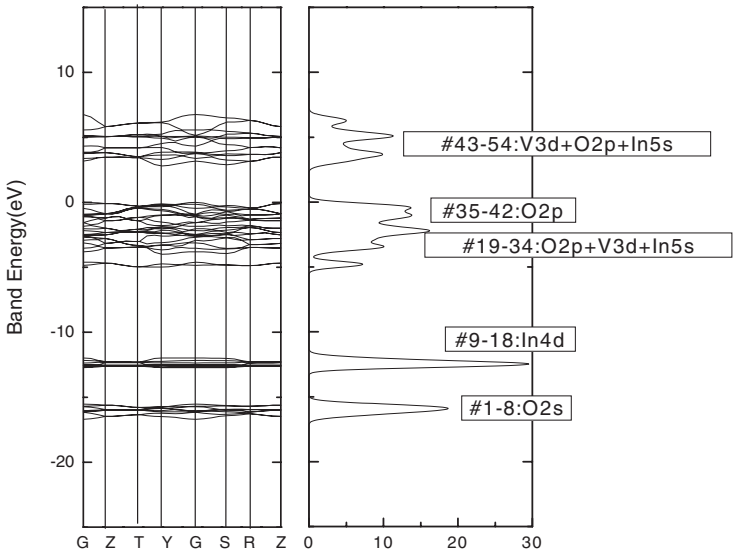

Fig. 6. The calculated band dispersions and densities of states for $InVO_4$.

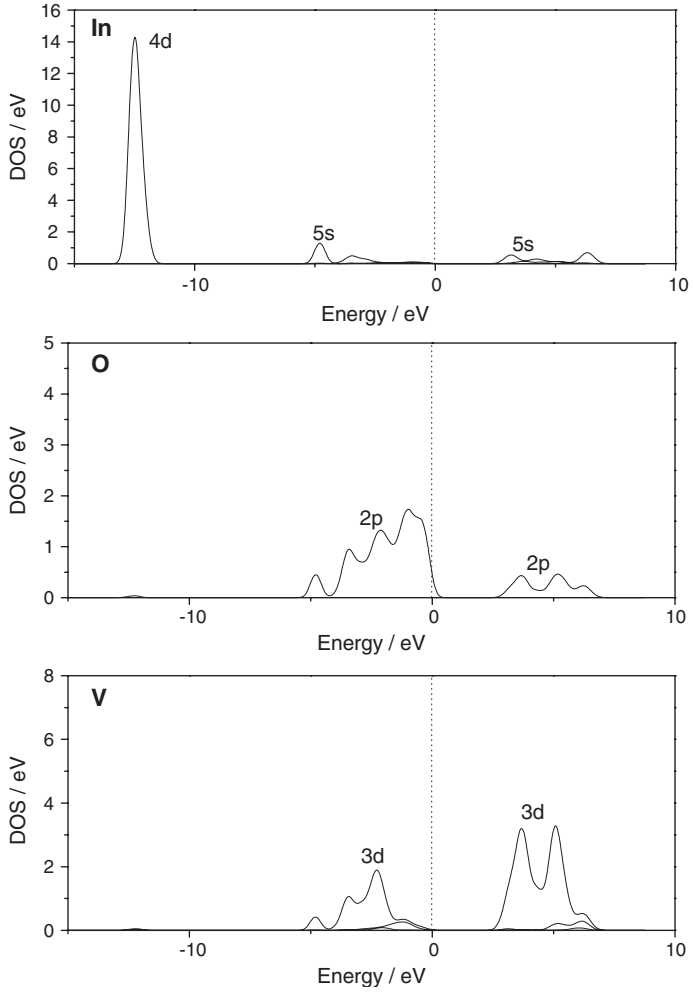

Fig. 7. The partial DOS for $InVO_4$.

density-functional-theory calculations is currently receiving increasing attention as a possible improvement over the LDA [32,33]. In Oshikiri's work, the band gap of $InVO_4$ was estimated to be 3.1 eV, compared with the experimental value (2.0 eV), the present work gave a more accuracy result (2.3 eV).

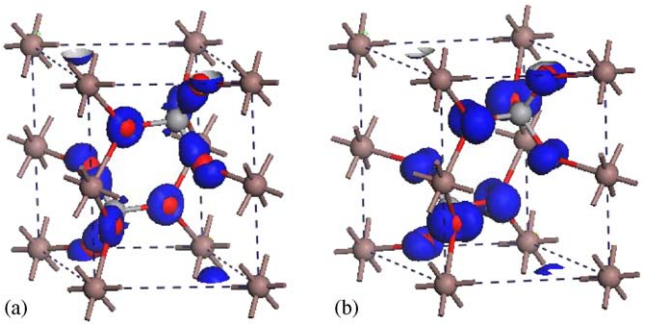

Fig. 8. Electron density contour map: (a) for band ♯30 of valence band (b) for the top of valence band (HOMO). Brown, grey and red balls represent In, V, and O atoms, respectively.

3.6. Photocatalysis activities

The photocatalytic activity of the $InVO_4$ nanoparticles was evaluated by degradation of FAD. Figs. 9 and 10 showed time profiles of C/C_0 under UV light and visible light irradiation ($\lambda > 420$ nm), where C was the concentration of FAD at the irradiation time t and C_0 was the concentration in the adsorption equilibrium on $InVO_4$ before irradiation. We prepared the $InVO_4$ by solid-state reaction using the same method in the reported literature [14]. $InVO_4$ showed activity in degradation of FAD both under UV light and visible light irradiation. The catalysts sintered from complex precursor showed higher activity than the one synthesized by solid-state reaction. The difference in the photocatalytic activity may partly be attributable to the fact that the powder via the complex precursor route has a nano-scale particle size, which means a relatively large surface area. Although owning different band gap energies, the catalyst obtained by calcining the complex precursor at 600 °C for various times exhibited almost the same photocatalytic activity, which could be attributed to their little difference in grain size and crystal size, as confirmed by TEM and XRD results (Table 2). However, when the calcining temperature rise to 700 °C, the sample shows a poor photocatalytic activity compared to the ones prepared at 600 °C. This can be explained by TEM results, which exhibited that the grain sizes grew quickly as the temperature increases.

In the synthesis of $InVO_4$, loss of vanadium is sensitive to the homogenerous extent of the distribution of metal ions in precursors for $InVO_4$. In the solid-state reaction methods, an inhomogeneous mixture comprised of coarse particles typically in the range of 1–10 μm is usually utilized. As the solid-state reaction relies on interdiffusion of the metals characterized by slow kinetics, a partial volatilization of vanadium components may occur during the heat-treatment at 1100 °C prior to the formation of the strictly stoichiometric $InVO_4$. A partial loss of vanadium should be responsible for the appearance of indium peaks as revealed by the XRD pattern. On the contrary, the constituent metal components are highly dispersed in the complex precursor in our method. The metal ions (mostly

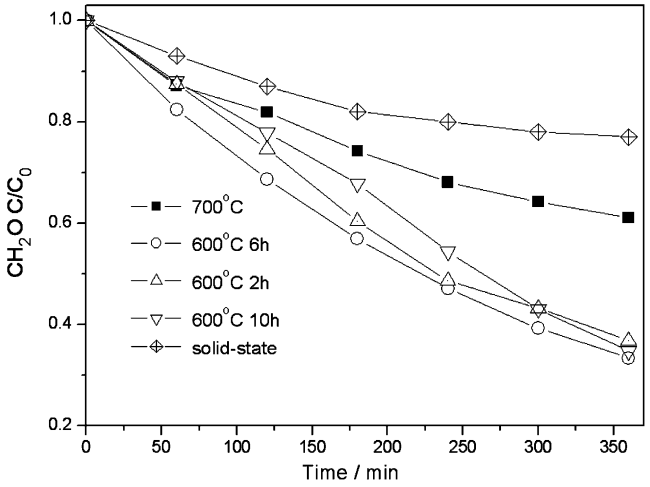

Fig. 9. The catalytic activity for photodecomposition of FAD under UV light irradiation over $InVO_4$ obtained by calcining the complex precursor and solid-state reaction at 1100 °C.

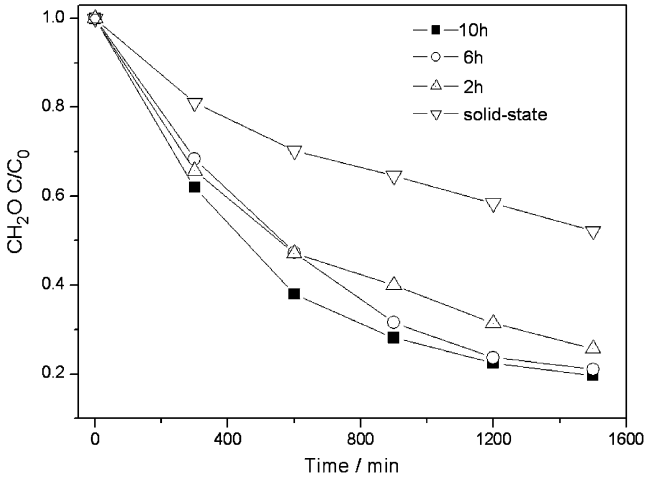

Fig. 10. The catalytic activity for photodecomposition of FAD under visible light irradiation over $InVO_4$ obtained by calcining the complex precursor at 600 °C for various times and solid-state reaction at 1100 °C.

complexed with DTPA) were immobilization in a rigid network. The contiguous ions of indium and vanadium in the resulting powder precursor can then react with each other with a minimum of diffusion at a relatively low temperature (600 °C) to form a homogeneous indium vanadate with a composition close to the stoichiometry.

4. Conclusions

In summary, $InVO_4$ nanoparticles have been obtained by calcining amorphous complex precursor at a relatively low temperature of 600 °C. The crystallinity, particle size, morphology, and photocatalytic activity of the $InVO_4$ nanoparticles can be modified easily by changing the calcination temperature and time. The $InVO_4$ nanoparticles showed higher photocatalytic activities under visible light irradiation ($\lambda > 420$ nm) than that of the sample

prepared by traditional solid-state reaction. This method has the potential use in preparation of other complex oxide photocatalysts powders and thin film photo-electrodes.

Acknowledgments

This work was partly supported by Chinese National Science Foundation (20433010, 20571047) and Trans-Century Training Program Foundation for the Talents by the Ministry of Education, PR China.

References

[1] M.R. Hoffmann, S.T. Martin, W. Choi, D.W. Bahnemann, Chem. Rev. 95 (1995) 69.
[2] M.A. Fox, M.T. Dulay, Chem. Rev. 93 (1993) 341.
[3] A.L. Linsebigler, G. Lu, J.T. Yates, Chem. Rev. 95 (1995) 735.
[4] M. Anpo, Res. Chem. Intermed. 11 (1989) 67.
[5] A. Kudo, K. Omori, H. Kato, J. Am. Chem. Soc. 121 (1999) 11459.
[6] S. Kohtani, M. Koshiko, A. Kudo, K. Tokumura, Y. Ishigaki, A. Toriba, K. Hayakawa, R. Nakagaki, Appl. Catal. B 46 (2003) 573.
[7] Z.G. Zou, J.H. Ye, K. Sayama, H. Arakawa, Nature 414 (2001) 625.
[8] M. Machida, J. Yabunaka, T. Kijima, Chem. Mater. 12 (2000) 812.
[9] J. Yin, Z.G. Zou, J.H. Ye, J. Phys. Chem. B 107 (2003) 61.
[10] J.W. Tang, Z.G. Zou, J.H. Ye, Chem. Mater. 16 (2004) 1644.
[11] J. Ye, Z. Zou, M. Oshikiri, A. Matsushita, M. Shimoda, M. Imai, T. Shishido, Chem. Phys. Lett. 356 (2002) 221.
[12] Z. Zou, J. Ye, K. Sayama, H. Arakawa, Chem. Phys. Lett. 343 (2001) 303.
[13] Z. Zou, J. Ye, K. Sayama, H. Arakawa, Chem. Phys. Lett. 333 (2001) 57.
[14] M. Touboul, P. Tole′dano, Acta Crystallogr. B 36 (1980) 240.
[15] M. Touboul, K. Melghit, P. Bénard-Rocherullé, Eur. J. Solid State Inorg. Chem. 31 (1994) 151.
[16] M. Guglielmi, G. Carturan, J. Non-Cryst. Solids 100 (1988) 16.
[17] Y. Suyama, A. Kato, J. Am. Ceram. Soc. 56 (1976) 146.
[18] S. Nishimoto, B. Ohtani, H. Kajiwara, T. Kajiya, J. Chem. Soc. Faraday Trans. 81 (1985) 61.
[19] A. Tsevis, N. Spanos, P.G. Koutsoukos, A.J. Linde, J. Lyklema, J. Chem. Soc. Faraday Trans. 94 (1998) 295.
[20] D.I. Roncaglia, I.L. Botto, E.J. Baran, J. Solid State Chem. 62 (1986) 10.
[21] Y.F. Zhu, T. Yi, S. Gao, C.H. Yan, L.L. Cao, J. Mater. Sci. 34 (1999) 4969.
[22] Y.F. Zhu, R.Q. Tan, T. Yi, S.S. Ji, X.Y. Ye, L.L. Cao, J. Mater. Sci. 35 (2000) 5415.
[23] T. Yi, S. Gao, X. Qi, Y.F. Zhu, F.X. Cheng, B.Q. Ma, Y.H. Huang, C.S. Liao, C.H. Yan, J. Phys. Chem. Solids 61 (2000) 1407.
[24] L. Wang, Y.F. Zhu, J. Alloys Comp. 370 (2004) 276.
[25] Judit Szanics, Masato Kakihana, Chem. Mater. 11 (1999) 2760.
[26] H. Wang, Y.F. Zhu, P. Liu, W.Q. Yao, J. Mater. Sci. 38 (2003) 1939.
[27] W. Kohn, L.J. Sham, Phys. Rev. A 140 (1965) 1133.
[28] J.P. Perdew, Y. Wang, Phys. Rev. B 45 (1992) 13244.
[29] M.C. Payne, M.P. Teter, D.C. Allan, T.A. Arias, J.D. Joannopoulos, Rev. Mod. Phys. 64 (1992) 1045.
[30] CASTEP Program is Developed and Distributed by Molecular Simulations Inc., San Diego, CA.
[31] M. Oshikiri, M. Boero, J. Ye, F. Aryasetiawan, G. Kido, Thin Solid Films 445 (2003) 168.
[32] J.P. Perdew, J.A. Chevay, S.H. Vosko, K.A. Jackson, M.R. Pederson, D.J. Singh, C. Fiolhais, Phys. Rev. B 46 (1992) 6671.
[33] B.G. Johnson, P.M.W. Gill, J.A. Pople, J. Chem. Phys. 98 (1993) 5612.